Earth and Planetary Science Letters 506 (2019) 104–112

Contents lists available at ScienceDirect

Earth and Planetary Science Letters

www.elsevier.com/locate/epsl

Uranium isotope evidence for an expansion of anoxia in terminal Ediacaran oceans

Rosalie Tostevin [a,b,*], Matthew O. Clarkson [c], Sophie Gangl [c], Graham A. Shields [d], Rachel A. Wood [e], Fred Bowyer [e], Amelia M. Penny [e], Claudine H. Stirling [c]

[a] University of Otago, Department of Geology, Dunedin 9016, New Zealand
[b] University of Oxford, Department of Earth Science, Oxford, OX1 3AN, UK
[c] University of Otago, Centre for Trace Element Analysis and Department of Chemistry, Union Place West, Dunedin 9016, New Zealand
[d] University College London, Department of Earth Sciences, Gower Street, London, WC1E 6BT, UK
[e] The University of Edinburgh, School of GeoSciences, James Hutton Road, EH9 3FE, Edinburgh, UK

ARTICLE INFO

Article history:
Received 29 August 2018
Received in revised form 25 October 2018
Accepted 29 October 2018
Available online 9 November 2018
Editor: L. Derry

Keywords:
redox
uranium
Ediacaran
oxygen
animals

ABSTRACT

Anoxic and iron-rich oceanic conditions prevailed throughout most of the Archean and Proterozoic (4000 to c.540 million years ago, Ma), but the oceans are hypothesised to have become progressively oxygen-rich during the Ediacaran–Cambrian transition interval, coincident with the rise of animal life. We utilise the uranium isotope ratio of seawater ($^{238}U/^{235}U$; reformulated as $\delta^{238}U$), an effective tracer of oceanic redox conditions, as a proxy for changes in the global proportion of anoxic seafloor. We present a new $\delta^{238}U$ dataset for carbonate rocks from the Lower Nama Group, Namibia, deposited in a shelf ramp succession during the terminal Neoproterozoic (~550 to ~547 Ma). These data capture a transition from $\delta^{238}U$ similar to the modern ocean towards persistently low $\delta^{238}U$ (average = −0.81 ± 0.06‰). Such low $\delta^{238}U$ are consistent with enhanced U drawdown from the water column under anoxic conditions, and the preferential export of 'heavy' ^{238}U to sediments following U(VI)–U(IV) reduction. Placing our results into a steady state ocean box model suggests at least a third of the global seafloor was covered by anoxic bottom waters compared with only 0.3% in today's oxygenated oceans. Comparison with $\delta^{238}U$ from older sediments deposited in other basins further supports an expansion of anoxic bottom waters towards the end of the Ediacaran. Our data are consistent with an emerging picture of a dominantly anoxic Ediacaran ocean punctuated by brief ocean oxygenation events. In the Nama Group, the transition towards globally widespread anoxic conditions post-dates the first appearance of both skeletal metazoans and soft-bodied fauna of the Nama Assemblage. This suggests that the global expansion of anoxia did not coincide with the decline of the Ediacaran biota, or drive the biotic turnover between the White Sea and Nama Assemblages. The impact of this global redox change on metazoan ecosystems is unclear, since the expansion of anoxia, if contained mainly within deeper waters, may not have impinged significantly upon continental shelves that host the majority of biodiversity.

1. Introduction

The oxygen-deficient Proterozoic oceans (2500 to c.540 million years ago, Ma) were characterised by ferruginous (anoxic and iron rich) conditions, with oxygenated surface waters and occasional euxinia (anoxia and free-H_2S) at mid-depths (Poulton and Canfield, 2011). The oceans are thought to have become progressively oxygenated in the Cryogenian, Ediacaran and Cambrian Periods (720–485 Ma), coincident with the rise of animal life (Canfield et al., 2007; Planavsky et al., 2014; Sahoo et al., 2012). However, the overall trend towards more oxygenated conditions has been difficult to constrain, because reconstructions have relied on localised redox proxies that record heterogeneous oceanic conditions among Neoproterozoic basins. Deepwater oxygenation has been recorded as early as 580 Ma in some basins, but others remained largely anoxic into the early Phanerozoic (Bowyer et al., 2017; Canfield et al., 2007; Wood et al., 2015). In particular, a recent compilation of Fe-speciation data, which records regional anoxia, from sediments deposited below storm wave base in multiple basins, finds no statistically significant trend towards oxygenation across the Ediacaran–Cambrian transition period (Sperling et al.,

* Corresponding author at: University of Oxford, Department of Earth Science, Oxford, OX1 3AN, UK.
E-mail address: Rosalie.tostevin@earth.ox.ac.uk (R. Tostevin).

https://doi.org/10.1016/j.epsl.2018.10.045
0012-821X/

2015). Together, this suggests that widespread deep water oxygenation did not occur until the Palaeozoic Era. However, such reconstructions based on localised redox proxies have only limited potential to constrain global trends in marine redox conditions due to incomplete coverage, bias in preserved facies, and hydrodynamic controls on local redox conditions that do not relate to changes in atmospheric oxygen levels.

Attempts to constrain the global extent of atmospheric and ocean oxygenation commonly are based on i) constraints on the burial of organic carbon and sulfide using carbon ($^{13}C/^{12}C$; $\delta^{13}C$) and sulphur isotopes ($^{34}S/^{32}S$; $\delta^{34}S$), ii) sedimentary enrichments or depletions in the redox-sensitive elements (e.g. uranium, vanadium, cerium, iodine and molybdenum), and iii) compositional shifts in various redox-sensitive metal stable isotope systems (e.g. chromium, selenium and molybdenum). However, these systems produce conflicting results for the onset of ocean oxygenation, with a very broad range that spans almost 300 Myr, from ca. 800 to 520 Ma (Fike et al., 2006; Kendall et al., 2015; Planavsky et al., 2014; Sahoo et al., 2012; Stolper and Keller, 2018). These conflicting findings may in part be due to the unique reduction potential of each system, each of which would have been surpassed progressively, and their different oceanic residence times which affect the timescale of response. Enrichments in redox sensitive trace metals in black shales suggest that rather than a single, unidirectional step change in oxygenation, the oceans instead remained broadly anoxic throughout the Neoproterozoic, but hosted a series of large perturbations, dubbed 'ocean oxygenation events (OOEs)' (Sahoo et al., 2016).

The timing of oceanic oxygenation is significant as it is hypothesised to have coincided with the rise of macroscopic metazoan life (Canfield et al., 2007). Body fossils of putative metazoans are first recorded ~571 Ma (Pu et al., 2016), but burrowing animals did not appear until after 560 Ma (Budd and Jensen, 2017). The earliest skeletal macrofossils appear globally ~550 Ma (Germs, 1983). The development of hard body parts is energetically costly, and explanations for the abrupt and globally synchronous emergence of biomineralisation have included ecological factors such as a rise in predation, and environmental factors, such an increase in alkalinity, or increased oxygen availability (Hua et al., 2003; Wood et al., 2017). Proxies that record the global extent of anoxia are required to investigate relationships between the innovation and distribution of biota, and major environmental change.

Using techniques in multiple-collector ICP-MS (MC-ICPMS) and double-spiking, we present coupled uranium isotope ($\delta^{238}U$) and U concentration (approximated by U/Ca) data preserved in carbonate rocks from the lower Nama Group, Namibia. Radiometric ages, as well as the presence of well-preserved biota, and globally correlative carbon isotope trends provide some constraints on the timing of deposition of the Nama Group (for geological and geochemical background, see SI-1). The integration of local and global redox proxies, in a section that directly preserves changes in biota, allows for co-interpretation without a need to correlate between possibly contemporaneous sections. These new results constrain global oceanic redox conditions spanning the interval from ~550–~547 Ma, and suggest anoxic bottom waters expanded to cover at least a third of the sea floor, following the emergence of the first skeletal animals and coincident with major perturbations in the sulphur and carbon cycles (Cui et al., 2016; Fike et al., 2006; Tostevin et al., 2017; Wood et al., 2015).

1.1. The uranium isotope paleo-redox proxy

Uranium primarily enters the ocean through riverine runoff, and in the modern ocean, U burial is split between sediments below anoxic bottom waters (20%), euxinic sediments below productive but oxygenated waters (23%), carbonates (23%), deltaic sediments (19%) and altered oceanic crust (10%) (Andersen et al., 2017; Dunk et al., 2002) (Fig. 1). Given that anoxic sediments account for less than 0.3% of the modern seafloor (Andersen et al., 2017; Dunk et al., 2002), U removal into anoxic sediments, which occurs via the reduction of highly soluble U(VI) to relatively insoluble U(IV), is disproportionately high. This makes the concentration of U in seawater very sensitive to the global extent of anoxia. Additionally, although the U isotope proxy has so far only been calibrated in modern euxinic settings, U reduction and removal should occur under all anoxic conditions. If this is the case, then U isotope systematics provide information on the total anoxic water mass. This differs from the isotope systematics of some other palaeoredox proxies which instead reflect the end-member redox state of anoxic and sulfidic conditions (e.g. Molybdenum).

In nature, the largest uranium isotope fractionations have been documented during oxidation–reduction associated with the U(VI)–U(IV) exchange reaction, resulting from variable nuclear volumes and electron density distributions between the different U isotopes (Abe et al., 2008). During the reduction of U(VI) to U(IV) under anoxic conditions, authigenic U enrichment occurs in the sediments as dispersed U(IV) precipitates (e.g. uranite), leaving the anoxic water column depleted in dissolved U. ^{238}U is preferentially removed into the sediments, leaving seawater depleted in this heavy isotope. The magnitude of this redox-related fractionation between ^{238}U and ^{235}U is at the permil-level (Stirling et al., 2007; Weyer et al., 2008), and dominates the U isotope signature of seawater.

In the modern environment, the $\delta^{238}U$ signature in seawater is well constrained ($-0.39 \pm 0.01‰$), and appears to be slightly lower than the mean signature of riverine input ($-0.26‰$) (Andersen et al., 2017; Stirling et al., 2007; Weyer et al., 2008). This is largely a result of ^{238}U–^{235}U fractionation during U burial in anoxic settings, despite these settings only accounting for a small proportion of the modern seafloor. Uranium has a long residence time in the modern ocean of ~400 ± 120 thousand years (kyr), and behaves conservatively (Dunk et al., 2002). The $\delta^{238}U$ of modern seawater is therefore globally homogeneous and captures changes in the strength of the anoxic sink over long timescales.

Uranium exists in seawater predominantly as the uranyl-tricarbonate ion [$UO_2(CO_3)_3^{4-}$], and this soluble form of uranium is directly incorporated into calcium carbonate. There is a growing body of evidence showing that, under most oceanic conditions, modern marine carbonate sediments preserve seawater $\delta^{238}U$ signatures ($\delta^{238}U_{SW}$) without large U isotope fractionations (Andersen et al., 2014; Chen et al., 2018; Romaniello et al., 2013; Stirling et al., 2007; Tissot and Dauphas, 2015; Weyer et al., 2008), provided minimal diagenetic exchange of the U isotopes has occurred following deposition. $\delta^{238}U$ in ancient carbonate rocks has therefore been successfully used as a global paleo-redox proxy (Andersen et al., 2014; Clarkson et al., 2018; Lau et al., 2017, 2016; Stirling et al., 2007; Zhang et al., 2018).

Early diagenesis has been observed to systematically drive $\delta^{238}U$ to higher values in some recent carbonates, especially those derived of primary metastable aragonite or aragonite–calcite mixtures, resulting in a positive offset from modern seawater of up to 0.3‰ (Romaniello et al., 2013). This offset is present in the majority of Holocene aragonitic sediments from the Bahamas, even those deposited below oxygenated bottom waters (Chen et al., 2018). As such, early diagenetic enrichments in ^{238}U with respect to ^{235}U cannot be easily detected using redox proxies such as Ce anomalies or Fe speciation (Chen et al., 2018; Hood et al., 2018). In addition, fabric specific work on Cryogenian carbonates has demonstrated that early cements, micrite and ooids may preserve primary $\delta^{238}U$ while microbialites and burial cements generally have altered $\delta^{238}U$ (Hood et al., 2018, 2016). However, if burial diagenesis is occurring under closed system conditions, the phase specific

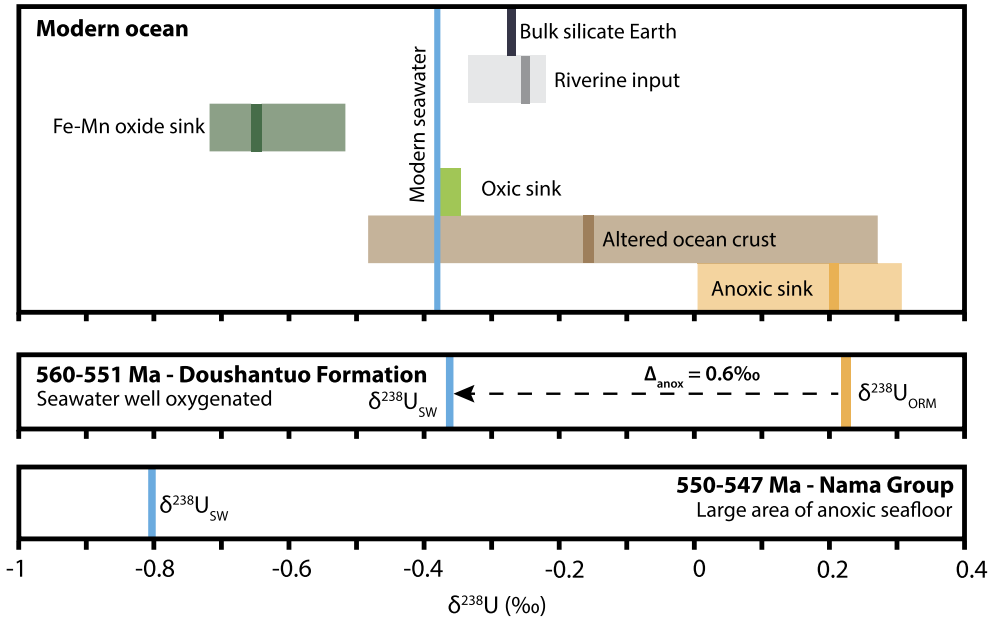

Fig. 1. Top panel: The range of $\delta^{238}U$ for different sources and sinks in the modern uranium cycle (Andersen et al., 2017, 2014; Stirling et al., 2007; Tissot and Dauphas, 2015; Weyer et al., 2008). Pale boxes define the potential range of values and solid boxes suggest the most likely value. Middle panel: The $\delta^{238}U$ of organic rich mudrocks in the Doushantuo Formation (Kendall et al., 2015), and the inferred $\delta^{238}U$ of seawater ($\delta^{238}U_{SW}$) using a fractionation factor between seawater and anoxic sediments (Δ_{anox}) of 0.6‰. Bottom panel: The $\delta^{238}U$ of carbonates from the Nama Group (this study), assumed to directly represent. For interpretation of the colours in the figure, the reader is referred to the web version of this article.

variability may be averaged, meaning the bulk rock values could still provide a reliable approximation of the initial primary signal.

2. Methods

The Nama Group, Namibia, is a mixed carbonate-siliciclastic sequence deposited in a ramp system, and exceptional exposure has allowed sequence stratigraphic, geochemical analysis and ecological surveys across multiple transects (see SI-1). Samples from a range of carbonate facies were selected from the Zebra River Section, which covers the Lower and Upper Omkyk, and Hoogland Members. The carbonates were probably originally deposited dominantly as aragonite, but have since neomorphosed to calcite. Dolomite-rich samples were excluded due to uncertainty surrounding the impact of dolomitisation on $\delta^{238}U$. $\delta^{13}C$ ($^{13}C/^{12}C$; reformulated as $\delta^{13}C$), $\delta^{18}O$ ($^{18}O/^{16}O$; reformulated as $\delta^{18}O$), $\delta^{34}S$ ($^{34}S/^{32}S$; reformulated as $\delta^{34}S$), major element, Fe-speciation and rare earth element data for the same samples, and the associated methods are published in Tostevin et al. (2017, 2016) and Wood et al. (2015).

All samples were prepared and analysed for their $\delta^{238}U$ composition at the Centre for Trace Element Analysis, University of Otago, New Zealand following protocols reported in SI-2. In brief, powders were subjected to a two-step reductive and oxidative cleaning procedure to remove potential Mn-oxides and residual organic matter (Clarkson et al., 2018). Carbonate was then selectively digested using a 1M sodium acetate buffer solution maintained at pH > 5, which avoids attacking the silicate fraction, as demonstrated by low Al concentrations (<20 ppm) (Table S2). The digest was resuspended in nitric acid and analysed via quadrupole ICP-MS to determine the concentrations of trace metals, including U and Ca. Based on the U concentration, leachates were subsampled to achieve a total U mass of 30–150 ng, and double spiked to give a $^{236}U/^{235}U$ ratio of approximately 3. Matrix elements (e.g. Na, Ca) were first removed through co-precipitation using pre-cleaned $FeCl_3$ and ammonia solution (Clarkson et al., 2018). The resulting precipitates were first dissolved in 6M HCl, and then resuspended in 3M HNO_3 and loaded onto heat shrink teflon columns containing UTEVA resin. Samples were then oxidised to eliminate any organic residues from the resin.

The purified U fractions were re-dissolved in 2% HCl and 0.01% HF, and analysed via MC-ICPMS. A ^{236}U–^{233}U double spike was used to correct for instrumental mass fractionation (Rolison et al., 2017; Stirling et al., 2007). The $^{238}U/^{235}U$ composition is presented in δ-notation following Eq. (1):

$$\delta^{238}U = \left(\frac{(^{238}U/^{235}U)_{sample}}{(^{238}U/^{235}U)_{CRM\text{-}145}} - 1 \right) \quad (1)$$

where CRM-145 is the 'zero-delta' standard. For a detailed method description, see SI-2 and references therein.

3. Results and assessment of diagenesis

U/Ca decreases up-section from scattered but generally higher values in the Lower Omkyk Member (average = 0.63 ± 0.28 μmol/mol (1 SE), range = 0.22 to 1.04 μmol/mol) to lower, more stable values in the Upper Omkyk and Hoogland Members (average = 0.21 ± 0.09 μmol/mol (1 SE), $n = 14$, range = 0.11 to 0.41 μmol/mol) (Fig. 2, Table S2). $\delta^{238}U$ decreases systematically from a maximum of −0.27‰ in the Lower Omkyk Member to a stable baseline of −0.81 ± 0.06‰ (1 SE) for the Upper Omkyk and Hoogland Members (excluding ZR29 at 168.1 m, with an outlying $\delta^{238}U$ of −0.48‰). One outlying sample (LO4 at 18 m) deviates from this trend and has a lower $\delta^{238}U$ than the adjacent samples of −0.97‰ (Fig. 2, Table S2). For a full assessment of the impacts of local water column redox conditions during deposition, facies control, early and late stage diagenesis, and detrital leaching, see SI-3 and SI-4.

There are several compelling reasons to suggest that the $\delta^{238}U$ in the Nama Group record a primary open ocean signature. Firstly, there is limited stratigraphic variability in $\delta^{238}U$ for the Upper Omkyk and Hoogland Members. Secondly, the rocks generally preserve primary marine geochemical signals based on other diagnostic parameters, including $\delta^{13}C$ and rare earth element patterns (Tostevin et al., 2016; Wood et al., 2015). Furthermore, the

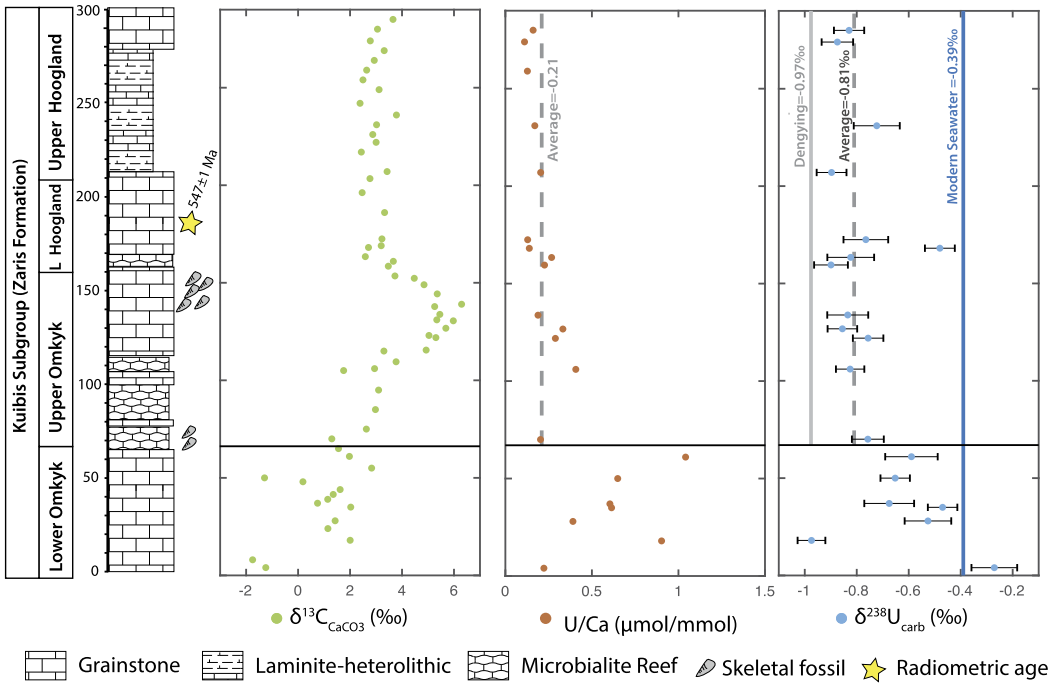

Fig. 2. Panels ordered left to right: Stratigraphic log, $\delta^{13}C$ (green circles), U/Ca ratios (orange circles) and $\delta^{238}U$ (blue circles) for carbonate rocks from Kuibis Subgroup of the Nama Group. The local distribution of biota within the section is marked on the stratigraphic log. The $\delta^{238}U$ of modern seawater (blue line) is shown for comparison. The average $\delta^{238}U$ (dashed grey line) is calculated as an average of all data in the upper Omkyk and Hoogland Members, excluding one anomalously enriched value. The $\delta^{238}U$ of contemporaneous carbonate rocks from the Dengying Formation, south China, are shown for comparison (solid grey line; Zhang et al., 2018).

co-occurring $\delta^{13}C$ is relatively enriched, suggesting minimal overprinting during meteoric diagenesis, and this is supported by petrographic analysis (Wood et al., 2018). While these parameters cannot be relied upon to identify alteration of $\delta^{238}U$, they suggest the Nama Group has the potential to preserve primary marine $\delta^{238}U$ (Chen et al., 2018; Hood et al., 2018). Thirdly, these samples have low TOC (<0.2 wt%) and were deposited under a locally oxygenated water column, and should therefore act as a passive sink for seawater U (Wood et al., 2015). Fourth, the Nama Group samples analysed here are composed of high purity samples (>90% $CaCO_3$) that preserve textural detail (Wood et al., 2018), indicating that neomorphism from primary aragonite occurred early and in the presence of fluids similar in composition to seawater. Finally, and most significantly, the Nama Group $\delta^{238}U$ closely matches pene-contemporaneous $\delta^{238}U$ from carbonates deposited in two independent sections from a geographically distant basin in South China (Zhang et al., 2018).

The $\delta^{238}U$ from south China display a similarly low $\delta^{238}U$ centred around -0.95 ± 0.10‰ and -0.97 ± 0.09‰ for Gaojiashan and Wuhe sections, respectively (Zhang et al., 2018), together confirming that low $\delta^{238}U$ is a primary global signal from the late Ediacaran. $\delta^{238}U$ from the oldest part of the Xiaotan section, south China reported in Wei et al. (2018) also capture the minima in $\delta^{238}U$ around -1‰. Additionally, the systematic trend towards lower $\delta^{238}U$ in the Lower Nama Group is also captured in equivalent sections from south China (Zhang et al., 2018). Zhang et al. (2018) screened their $\delta^{238}U$ data using a number of geochemical criteria, including Mn/Sr ratios <2.5, although there is no evidence to suggest that Mn/Sr cut-offs can be reliably used to screen for alteration of $\delta^{238}U$ in bulk carbonate rocks (Chen et al., 2018). In Fig. 3, we plot the un-screened $\delta^{238}U$ for comparison, and the trend from near-modern $\delta^{238}U$ to very low $\delta^{238}U$ is apparent in all three sections.

Despite similar trends, the Nama Group does not appear to record the minima in $\delta^{238}U$ observed in south China. While there are numerous lines of evidence to suggest the Lower Nama Group and the Dengying Formation were deposited at similar times, including capturing similar $\delta^{13}C$ and $\delta^{34}S$, the presence of the Nama biota, and overlapping radiometric dates, there is some uncertainty in dating and correlations that mean the sections could either be contemporaneous or very close in age (Cui et al., 2016; Tostevin et al., 2017; Zhang et al., 2018). If the Nama Group was deposited slightly earlier than the Dengying, it may not record the full breadth of the transition to a very low $\delta^{238}U$ of around -1‰. Alternately, if the sections were deposited at precisely the same time, then there may be a diagenetic offset of 0.1–0.2‰ in the Nama section (see full discussion of diagenetic effects in SI-3, SI-4 and Fig. S1). Since diagenetic alteration in shallow modern carbonate sediments generally results in higher $\delta^{238}U$ (Chen et al., 2018; Hood et al., 2018), the minimum values recorded globally may be more representative of seawater signatures. This suggests that the lowest $\delta^{238}U$ as recorded in south China might be closest to seawater $\delta^{238}U$ for the latest Ediacaran.

4. Discussion

4.1. Ediacaran seawater $\delta^{238}U$

There are some higher $\delta^{238}U$ in the Lower Omkyk Member (up to -0.27‰) which give rise to an apparent systematic, secular trend of decreasing $\delta^{238}U$ up section towards a baseline of -0.81 ± 0.06‰ in the Upper Omkyk and Hoogland Members. This $\delta^{238}U$ baseline sits 0.43‰ below the $\delta^{238}U$ of modern seawater and may represent a maximum estimate of seawater $\delta^{238}U$ at the time of deposition. If we assume that the higher $\delta^{238}U$ and generally higher U/Ca represents a primary signal, these trends can be interpreted to reflect the progressive removal of U from the water column and preferential export of heavy ^{238}U to sediments under expanding seafloor anoxia in the latest Ediacaran. Primary trends in the Lower Omkyk Member of the Nama Group are supported by comparisons with the $\delta^{238}U$ of organic-rich mudrocks ($\delta^{238}U_{ORM}$) from Member IV of the Doushantuo Formation, South China (Kendall et al., 2015), deposited immediately before the Nama Group at 560–551 Ma. The $\delta^{238}U_{SW}$ for this time pe-

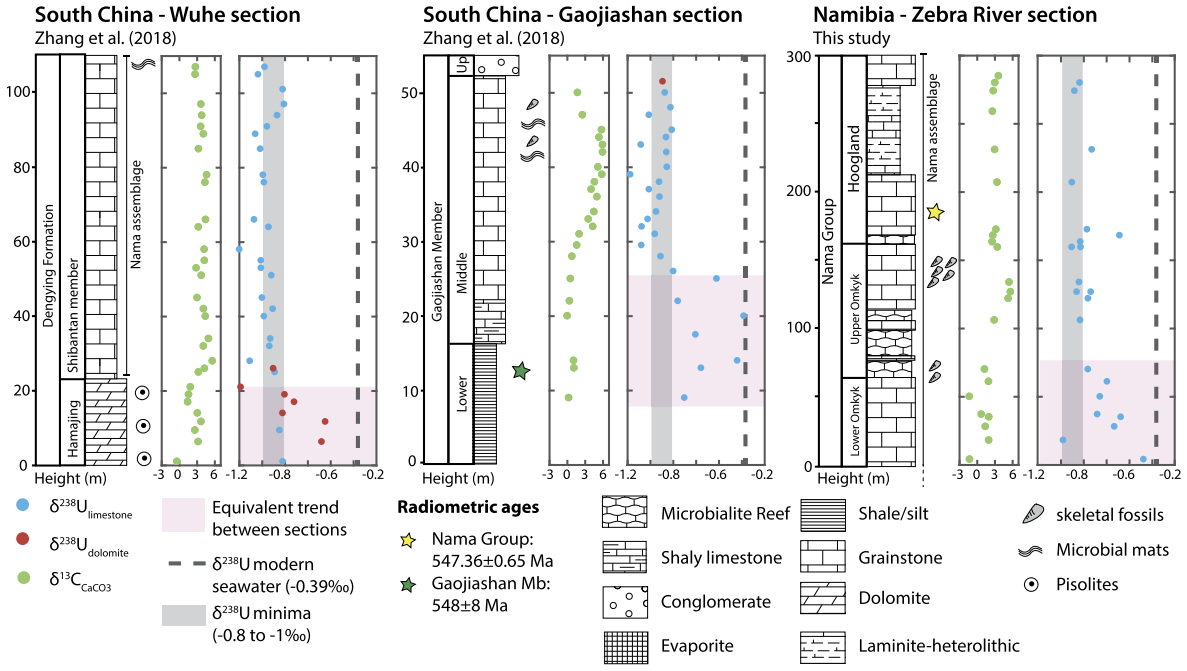

Fig. 3. Comparison of $\delta^{13}C$ and $\delta^{238}U$ from the Nama Group, Namibia (this study), with two independent carbonate sections of the Dengying Formation, south China (Wuhe and Gaojiashan) (from Zhang et al., 2018). The trend from modern marine $\delta^{238}U$ (black dashed line) towards low $\delta^{238}U$ of −0.8 to −1.0‰ (grey line) is apparent in all three sections, in both limestone and dolostone. The stratigraphic log for Gaojiashan is based on Cui et al. (2016). The recorded range of the Nama Assemblage is indicated on the stratigraphic log, with dashed lines indicating that the range extends below the base of the section.

riod can be calculated from the $\delta^{238}U_{ORM}$, using an assumed U isotope fractionation factor between seawater and the anoxic sinks of 0.6‰ (Kendall et al., 2015). This gives an average $\delta^{238}U_{SW}$ of −0.34 ± 0.11‰ (excluding anomalously low values at the top of the cores) which is within error of the modern ocean value of −0.39 ± 0.01‰ (Andersen et al., 2017, 2014; Rolison et al., 2017; Tissot and Dauphas, 2015). This result was interpreted as indicating widespread marine oxygenation, and is supported by oxygenated signals from molybdenum (Mo) isotopic signatures on the same samples.

The decrease in average $\delta^{238}U_{SW}$ from −0.34‰ to −0.81‰, obtained by combining the average $\delta^{238}U$ during Doushantuo deposition (~560 to ~551 Ma) with the average $\delta^{238}U$ during Nama Group deposition (~550 to ~547 Ma), implies increased U(IV) removal from seawater and the preferential export of heavy ^{238}U from the water column around 550 Ma (Figs. 1 and 4). Lower $\delta^{238}U_{ORM}$ of −1.02‰ observed in the youngest rocks of the Doushantuo cores (Kendall et al., 2015) could indicate the onset of this anoxia expansion, and be equivalent to the apparent secular trends seen in the lower Nama Group and Dengying Formation (Zhang et al., 2018). Further, U/TOC in Member IV of the Doushantuo Formation supports declining U concentrations ~550 Ma (Sahoo et al., 2016), consistent with declining average U/Ca across the Lower Nama Group, suggesting U drawdown under expanded ocean anoxia. Overall, the trends in $\delta^{238}U$ and U/Ca in the Nama Group, when compared with $\delta^{238}U$ from the Doushantuo Formation and the Dengying Formation, fit well with global trends and support a rapid and dramatic decrease in $\delta^{238}U$ around 550 Ma (Fig. 4).

4.2. Constraining the extent of anoxia during the Ediacaran

Low $\delta^{238}U_{SW}$ is broadly consistent with an expansion of seafloor anoxia, and we use an ocean box model to explore the implications of a $\delta^{238}U_{SW}$ of −0.81‰ for the Ediacaran ocean redox state after Zhang et al. (2018), as follows:

$$\delta^{238}U_{SW} = \frac{[\delta^{238}riv - (A_{anox} * k_{anox} * \Delta_{anox}) + (A_{low} * k_{low} * \Delta_{low}) + (A_{oxic} * k_{oxic} * \Delta_{oxic})]}{(A_{anoxic} * k_{anoxic}) + (A_{low} * k_{low}) + (A_{oxic} * k_{oxic})} \quad (2)$$

For a full description of the model structure and derivation of equation (1), see SI-5. In equation (1), $\delta^{238}U_{riv}$ is the modern riverine $\delta^{238}U$, prescribed here as $\delta^{238}U_{riv} = -0.30‰$, consistent with previous models and the average for upper continental crust (−0.29 ± 0.06‰) (Andersen et al., 2017; Montoya-Pino et al., 2010; Zhang et al., 2018). Variable k is the effective burial rate constant for each of the three burial sinks, and is derived by inverting the area and burial fluxes of U in modern environments (Zhang et al., 2018). The model assumes that uranium enters the ocean through rivers, and leaves via three major sinks: sediments below anoxic, low oxygen or oxic bottom waters. Here, low oxygen is defined as deposition below bottom waters containing 0.2–2 ml/L of dissolved O_2 and the anoxic sink includes deposition below both anoxic ferruginous and euxinic waters. The oxic sink is an amalgamation of several minor sinks, including Fe–Mn crusts, carbonate sediments, pelagic clays, alteration of oceanic crust, and coastal retention. The U isotope fractionation associated with the oxic and low oxygen sinks is small (0.005‰ and 0.1‰ respectively; Andersen et al., 2017). We take the U isotope fractionation factor between seawater and anoxic sinks, Δ_{anox}, to be 0.6‰ (Andersen et al., 2014; Rolison et al., 2017). The area of anoxic, low oxygen and oxic seafloor (A_{anox}, A_{low} and A_{oxic}) is determined by the total area of seafloor ($A_{ocean} = 3.61 * 10^{16}$ dm^2) multiplied by the fraction of seafloor covered by anoxic (F_{anox}), low oxygen (F_{low}) or oxic (F_{ox}) bottom waters, respectively. F_{anox} is allowed to vary between 0 and 1. F_{low} covaries with F_{ox} and is assumed to remain 6% of the size of the oxic sink, consistent with modern environments.

Expanding ocean anoxia drives $\delta^{238}U_{SW}$ lower. To generate a $\delta^{238}U_{SW}$ of −0.81‰ requires a large area of seafloor anoxia of 33%. The model is very insensitive at low $\delta^{238}U_{SW}$, such that a large change in seafloor anoxia is required to drive a small change in the resulting U isotope value (Lau et al., 2017). This means that the

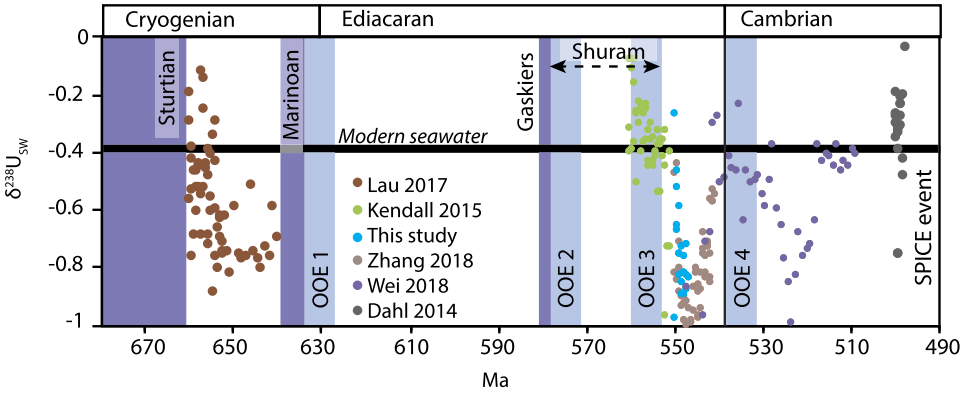

Fig. 4. Compilation of limited $\delta^{238}U_{SW}$ inferred from Neoproterozoic and Cambrian rocks (Dahl et al., 2014; Kendall et al., 2015; Lau et al., 2017; Wei et al., 2018; Zhang et al., 2018). The transition from a modern marine $\delta^{238}U_{SW}$ to much lower $\delta^{238}U_{SW}$ ~550 Ma coincides with the end of an inferred 'ocean oxygenation event (OOE)' (pale blue panels, Sahoo et al., 2016). Data from Kendall et al. (2015) has been replotted as $\delta^{238}U_{SW}$ using an assumed U isotope fractionation factor between anoxic sediments and seawater of 0.6‰, consistent with Kendall et al. (2015). Global or expansive periods of glaciation are also marked in purple.

small variations in $\delta^{238}U_{SW}$ through the section, and uncertainty about the extent of diagenetic enrichment, have large implications for the calculated area of anoxic seafloor. Given diagenetic enrichments may have skewed the Nama Group to higher $\delta^{238}U$, 33% represents a minimum estimate of seafloor anoxia. Under the conditions described above, the model cannot reproduce the very low $\delta^{238}U$ of −0.97‰ recorded in south China. However, the model is sensitive to the U isotope fractionation factor associated with the anoxic sink, the assumed k function, and, to a lesser extent, the $\delta^{238}U$ of riverine input. We explore the sensitivity of our model to these parameters below (see Table 1).

The $\delta^{238}U$ of modern rivers varies widely, depending on the geology of the catchment area, since evaporites, limestones, dolomites, granites and black shales all have unique $\delta^{238}U$ (Andersen et al., 2017; Stirling et al., 2007; Tissot and Dauphas, 2015). However, a weighted mean of all surveyed rivers gives a $\delta^{238}U_{riv}$ of −0.34‰, but this average is strongly influenced by one exceptionally low $\delta^{238}U$ reported from the Yangtze river (−0.70‰). If this river is excluded from the calculation, the global mean riverine $\delta^{238}U$ is −0.26‰ (Andersen et al., 2017). In general, lower $\delta^{238}U_{riv}$ results in a smaller estimate of the area of anoxic seafloor. For example, for a higher $\delta^{238}U_{riv}$ of −0.26‰ a larger expanse of anoxic seafloor is required to explain the Nama Group data (55%). Conversely, for a $\delta^{238}U_{riv}$ of −0.34‰, a reduced extent of anoxic seafloor is implied (24%). Changes in $\delta^{238}U_{riv}$ within this range can not drive $\delta^{238}U_{SW}$ to the low values recorded in south China (−0.97‰), even with 100% sea floor anoxia (Fig. 5a).

Of all the fractionations involved in the U isotope system, those associated with the anoxic sink are the largest but remain under constrained. Our model is highly sensitive to the assumed fractionation factor, with a smaller Δ_{anox} implying a greater extent of anoxia for a given $\delta^{238}U_{SW}$. We test the sensitivity of our model to extreme high and low fractionation factors between 0.5 and 1.2‰ (Fig. 5b). For example, a larger Δ_{anox}, of 0.7‰, can be reconciled with our data with 18% of the seafloor covered by anoxic bottom waters, whereas a smaller Δ_{anox}, of 0.5 cannot be reconciled with our data, even if 100% of the seafloor is anoxic (Fig. 5). For a δ^{238}Uriv of −0.30‰, a minimum Δ_{anox} of 0.67‰ is required to produce a $\delta^{238}U_{SW}$ of −0.97‰, as recorded in south China (Zhang et al., 2018). The model is extremely sensitive to the assigned global average k_{anox} and Δ_{anox}, but both of these values are based on fluxes in isolated modern anoxic water bodies such as the Black Sea and the Cariaco Basin. It is not clear whether these values can be extrapolated to the past global ocean with very high A_{anox}. Further U isotope studies of modern anoxic and euxinic basins are required to continue to refine the magnitude of k_{anox} and Δ_{anox}, particularly under the anoxic ferruginous conditions that may have typified Ediacaran oceans (Rolison et al., 2017).

Regardless of the sensitivity of the model to various poorly constrained fluxes and $\delta^{238}U$, our data cannot be explained simply by variation in the riverine composition or the U isotope fractionation factor between anoxic sediments and seawater (Δ_{anox}). Importantly, only changing the size of the anoxic sink is able to drive the δ^{238}Usw to the very negative values observed in the Nama group, although uncertainties in riverine $\delta^{238}U$ and Δ_{anox} will impact the scale of anoxic expansion required to explain the data. The only way to reconcile our U isotope data with those from 560–550 Ma is a dramatic expansion of marine anoxia from near-modern levels to between 24% and 100% of the seafloor.

4.3. Neoproterozoic redox conditions

The new $\delta^{238}U$ and U/Ca records presented here, considered in a global context, suggest that there was a rapid and dramatic increase in the extent of seafloor anoxia around 550 Ma (Kendall et al., 2015; Wei et al., 2018; Zhang et al., 2018) (Figs. 4 and 5). This transition coincides with a small positive carbon isotope excursion (Fig. 3, Cui et al., 2016; Zhang et al., 2018), indicating enhanced carbon burial under anoxic conditions. A shift in the marine sulphur cycle, recorded by $\delta^{34}S$, occurs around the same time, possibly consistent with more widespread sulfate reduction under anoxic conditions (Cui et al., 2016; Fike et al., 2006; Tostevin et al., 2017). Certainly, U reduction mediated by sulfate-reducing bacteria under anoxic conditions is known to drive U isotope fractionation of the direction and magnitude captured by the Nama Group (Andersen et al., 2017; Stirling et al., 2015; Stylo et al., 2015). One possibility is that the combined $\delta^{238}U$ and $\delta^{34}S$ data capture an intriguing link between the sulphur and uranium cycles, reflecting increased euxinia in the latest Ediacaran. The transition to higher $\delta^{34}S$ may additionally reflect an elevated riverine flux or changing riverine source, suggesting a link between changes in weathering regimes and the type and extent of anoxia (Cui et al., 2016).

Widespread anoxia within ten million years of the Ediacaran–Cambrian boundary is consistent with recent compilations of Fe-speciation data which show no overall trend towards oxygenation in the Neoproterozoic (Sperling et al., 2015); $Fe^{3+}/\sum Fe$ ratios in submarine basalts which place deep ocean oxygenation in the Late Palaeozoic (Stolper and Keller, 2018); biogeochemical models which predict a rise in oxygen around 400 Ma (Bergman et al., 2004), as well as molybdenum isotope data which place the oxygenation of the oceans in the Palaeozoic (~520 to 400 Ma) (Chen et al., 2015). In addition, earlier work based on Th/U ra-

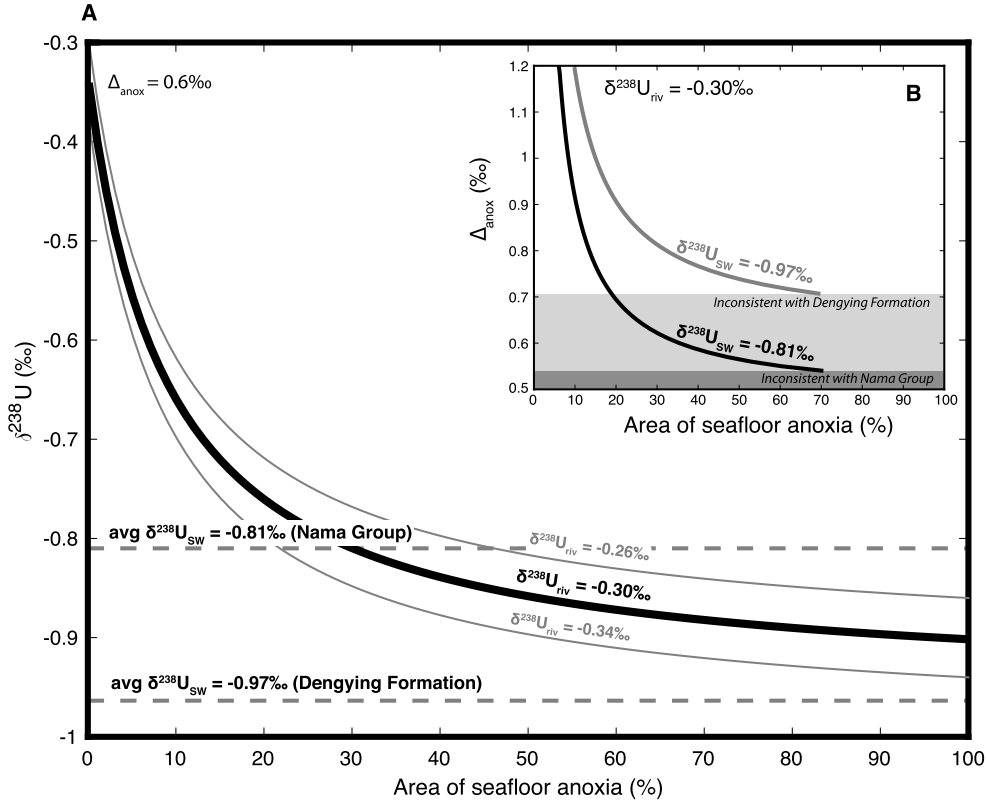

Fig. 5. a) Model results for the $\delta^{238}U_{SW}$ resulting from a given percentage of anoxic seafloor based on Δ_{anox} = 0.6‰ and $\delta^{238}U_{riv}$ of −0.30‰. A lower $\delta^{238}U_{riv}$ of −0.34‰ results in a smaller estimate of seafloor anoxia, and a higher $\delta^{238}U_{riv}$ of −0.26‰ results in a larger estimate of seafloor anoxia. b) For lower Δ_{anox}, a greater increase in seafloor anoxia (F_{anox}) is required to reproduce $\delta^{238}U_{SW}$ of −0.81‰ recorded in the Nama Group. The average $\delta^{238}U$ recorded in the Dengying Formation, south China, is shown for comparison (Zhang et al., 2018).

Table 1
Parameters, symbols and selected values used in the steady state model. Values in brackets are the ranges considered in sensitivity tests.

Parameter	Symbol	Value	Reference
$\delta^{238}U$ of global riverine input	$\delta^{238}U_{riv}$	−0.30‰ (−0.34 to −0.26‰)	Andersen et al., 2017
$\delta^{238}U$ of Ediacaran seawater	$\delta^{238}U_{SW}$	−0.81‰ to 0.89‰	
Isotope fractionation between seawater and oxic sinks	Δ_{oxic}	0.005‰	Weyer et al., 2008
Isotope fractionation between seawater and low oxygen sinks	Δ_{low}	0.1‰	Tissot and Dauphas, 2015
Isotope fractionation between seawater and anoxic sinks	Δ_{anox}	0.6‰ (0.5–1.2‰)	Andersen et al., 2017; Weyer et al., 2008
Fraction of seafloor overlain by oxic bottom waters	F_{oxic}	$= 1 - F_{low} - F_{anox}$	
Fraction of seafloor overlain by low oxygen bottom waters	F_{low}	0.06 until F_{anox} >0.94, then $F_{oxic} = 0$ and $F_{low} = 1 - F_{anox}$	
Fraction of seafloor overlain by anoxic bottom waters	F_{anox}	0–1	
Total area of ocean floor	A_{ocean}	3.61E16 dm^2	
Effective burial rate constant for oxic sinks	k_{oxic}	0.0536 dm/yr	Dunk et al., 2002
Effective burial rate constant for low oxygen sinks	k_{low}	0.469 dm/yr	Dunk et al., 2002
Effective burial rate constant for anoxic sinks	k_{anox}	0.939 dm/yr	Zhang et al., 2018

tios suggests the Precambrian–Cambrian boundary was associated with the widespread development of anoxic shallow marine environments (Kimura and Watanabe, 2001). Together, this evidence suggests that there was no unidirectional change in marine oxygenation during the Neoproterozoic, and instead that the oceans remained broadly anoxic until later in Earth's history. Although the relationship between local and global oceanic redox conditions is complex, local redox proxy data are consistent with heterogeneous, poorly ventilated basins at ~550 Ma (Bowyer et al., 2017; Sperling et al., 2015; Wood et al., 2015).

Sahoo et al. (2016) proposed a series of ocean oxygenation events (OOEs) within the broadly anoxic Neoproterozoic ocean. A compilation of $\delta^{238}U_{SW}$ across the Neoproterozoic and early Palaeozoic (Fig. 4) reveals dramatic oscillations that coincide with proposed OOEs. Our data could capture the end of OOE 3, ~560 Ma, and the transition back to widespread anoxia (Fig. 4). $\delta^{238}U$ data from the Yanjiahe Formation and Zhujiaqiang Formation in south china highlight another oxygenation event (OOE 4), at the base of the Cambrian, followed by a slow return to global anoxia (Wei et al., 2018). Similarly, $\delta^{238}U$ data as well as trace metal enrichments record a brief oxygenation event after the Sturtian glaciation (650–630 Ma), followed by a return to anoxic conditions (Lau et al., 2017; Sahoo et al., 2012; Fig. 4). It appears that oceanic redox conditions oscillated dramatically several times before any permanent switch to a new stable oxygenated state occurred, but the driver for such rapid and global change remains enigmatic. One possibility is that step changes in the burial of phosphorus and organic carbon, driven by evolutionary innovations, progressively lowered marine phosphate levels. Each step change would result in a pulse of marine oxygena-

tion, but over long timescales the decrease in C_{org}/P burial ratios would drive atmospheric oxygen levels down, and slowly deoxygenate the oceans (Lenton and Daines, 2018). One possible evolutionary driver is the onset of increasingly complex bioturbation during the late Ediacaran and Cambrian. Fine meiofaunal traces, capable of disrupting the sediment-mat interface, appeared after 560 Ma, coincident with OOE 3 (Budd and Jensen, 2017; Lenton and Daines, 2018). The onset of more complex forms of burrowing, including shallow penetrative burrows, appears close to the Cambrian boundary, and could be the driver for OOE 4 (Jensen et al., 2000).

4.4. Implications for early animal ecosystems

Widespread anoxia may present both a challenge and an opportunity for marine ecosystems (Wood and Erwin, 2017). Anoxia can drive mass extinctions, through habitat loss or contraction as well as indirect effects on nutrient availability (Hull et al., 2015). But by removing incumbents, mass extinction events disrupt established ecological niches, leaving them open for new taxa to colonise (Hull et al., 2015). There is evidence around 550 Ma for a biotic turnover and reduction in diversity between the soft bodied macrobiotas known as the White Sea and Nama Assemblages (Waggoner, 2003). The Nama Assemblage, however, also marks a diversification of bilaterian trace fossils (Tarhan et al., 2018), and the emergence of new innovations including metazoan biomineralization (Germs, 1983). A global expansion of anoxia has been proposed to coincide with decline of the Ediacaran biota around 550 Ma (Zhang et al., 2018).

The Nama Group is relatively well dated radiometrically and hosts skeletal as well as soft-bodied biota from the Nama Assemblage. Our integrated data demonstrate that the transition towards globally widespread anoxic conditions post-dates both the first appearance of the Nama Assemblage, and skeletal metazoans. Soft-bodied biota belonging to the Nama Assemblage are recorded in the Kanies Member (Bowyer et al., 2017), which sits stratigraphically below the lower Omkyk Member so pre-dating the $\delta^{238}U$ transition to expanded anoxia. Skeletal *Cloudina* is present in the Mara Member (Germs, 1983), which was deposited coincident with the Kanies Member and the lower part of the Lower Omkyk Member, and so predates the $\delta^{238}U$ minima. These data show that the global expansion of anoxia cannot have driven the decline in the Ediacaran biota or biotic turnover. They may, instead, reflect a geochemical response to ecological change (Lenton and Daines, 2018).

Following the global expansion of anoxia, our model suggests that more than a third of the sea floor was covered by anoxic bottom waters. However, there is no evidence that this transition impacted on the diversity or distribution of biota within the Nama Group (Bowyer et al., 2017). Expanded anoxia does not necessarily have to restrict shallow habitable space, if the oxygen minimum zone expands downwards into deeper waters. Modern continental shelf settings (defined as shallower than 150 m) make up less than 10% of the modern sea floor, and yet host the majority of benthic biodiversity. The abyssal plain, in contrast, comprises over 70% of the sea floor. The Nama Group records a continental shelf ramp system with no basinal facies, so it is possible that a global expansion of seafloor anoxia, if contained within deeper waters, did not impinge on shallow shelf communities. The Nama Group, therefore, demonstrates that complex metazoan communities can thrive in locally well-oxygenated niches despite globally widespread anoxia (Tostevin et al., 2016; Wood et al., 2015).

5. Conclusions

We present a new $\delta^{238}U$ dataset from carbonate rocks from the Nama Group, Namibia, deposited at ~550–547 Ma. We report a transition from a U isotope signature equivalent to the modern marine $\delta^{238}U$, to much lower $\delta^{238}U$, reaching an average of $-0.81 \pm 0.06‰$. Correlations between $\delta^{238}U$ and other global sections indicate this average could represent a maximum estimate of $\delta^{238}U_{SW}$. Comparison with $\delta^{238}U$ observations from black shales in directly underlying strata from south China further supports a dramatic shift in $\delta^{238}U_{SW}$ around ~550 Ma. We use a mass balance model to explore the implications of this $\delta^{238}U$ transition, and find that oceanic conditions must have switched from broadly oxygenated (with <0.3% of the seafloor covered by anoxic bottom waters) to having widespread anoxic bottom waters (at least a third of the seafloor). Integrated geochemical and biotic records reveal that the redox transition post-dates the first appearance of skeletal fauna and soft-bodied biota belonging to the Nama Assemblage. These data conclusively demonstrate that expanded anoxia cannot have driven the biotic turnover between the White Sea and Nama Assemblages, and may instead be a response to ecological change.

Author contributions

RT, FB, AMP and RW collected the samples. RT prepared the samples with assistance from MOC, SG and CHS. RT created the model with MOC. RT interpreted the data and drafted the manuscript with input from all co-authors.

Acknowledgements

We thank Chris Reinhard, one anonymous reviewer and editor Lou Derry for their detailed and thoughtful suggestions. R.T., M.O.C., S.G. and C.H.S., were supported by the Royal Society of New Zealand, Marsden Fund Standard Grant UOO1314. RT, GAS and RAW acknowledge financial support from NERC's Life and the Planet project (NE/1005978/1). We are grateful to L. and G. Fourie for access to Zebra River farm, and Gerd Winterleitner for help with field work. Thank you to David Barr and Malcolm Reid for support in the lab.

Appendix A. Supplementary material

Supplementary material related to this article can be found online at https://doi.org/10.1016/j.epsl.2018.10.045.

References

Abe, M., Suzuki, T., Fujii, Y., Hada, M., Hirao, K., 2008. An ab initio molecular orbital study of the nuclear volume effects in uranium isotope fractionations. J. Chem. Phys. 129, 164309. https://doi.org/10.1063/1.2992616.

Andersen, M.B., Romaniello, S., Vance, D., Little, S.H., Herdman, R., Lyons, T.W., 2014. A modern framework for the interpretation of $^{238}U/^{235}U$ in studies of ancient ocean redox. Earth Planet. Sci. Lett. 400, 184–194. https://doi.org/10.1016/j.epsl.2014.05.051.

Andersen, M.B., Stirling, C.H., Weyer, S., 2017. Uranium isotope fractionation. Rev. Mineral. Geochem. 82, 799–850. https://doi.org/10.2138/rmg.2017.82.19.

Bergman, N.M., Lenton, T.M., Watson, A.J., 2004. COPSE: a new model of biogeochemical cycling over Phanerozoic time. Am. J. Sci. 304, 397–437.

Bowyer, F., Wood, R.A., Poulton, S.W., 2017. Controls on the evolution of Ediacaran metazoan ecosystems: a redox perspective. Geobiology 15, 516–551. https://doi.org/10.1111/gbi.12232.

Budd, G.E., Jensen, S., 2017. The origin of the animals and a 'Savannah' hypothesis for early bilaterian evolution. Biol. Rev. 92, 446–473. https://doi.org/10.1111/brv.12239.

Canfield, D.E., Poulton, S.W., Narbonne, G.M., 2007. Late-neoproterozoic deep-ocean oxygenation and the rise of animal life. Science 315, 92–95. https://doi.org/10.1126/science.1135013.

Chen, X., Ling, H.-F., Vance, D., Shields-Zhou, G.A., Zhu, M., Poulton, S.W., Och, L.M., Jiang, S.-Y., Li, D., Cremonese, L., Archer, C., 2015. Rise to modern levels of ocean oxygenation coincided with the Cambrian radiation of animals. Nat. Commun. 6. https://doi.org/10.1038/ncomms8142.

Chen, X., Romaniello, S.J., Herrmann, A.D., Hardisty, D., Gill, B.C., Anbar, A.D., 2018. Diagenetic effects on uranium isotope fractionation in carbonate sediments from the Bahamas. Geochim. Cosmochim. Acta 237, 294–311. https://doi.org/10.1016/j.gca.2018.06.026.

Clarkson, M.O., Stirling, C.H., Jenkyns, H.C., Dickson, A.J., Porcelli, D., Moy, C.M., von Strandmann, P.A.E.P., Cooke, I.R., Lenton, T.M., 2018. Uranium isotope evidence for two episodes of deoxygenation during Oceanic Anoxic Event 2. Proc. Natl. Acad. Sci., 201715278. https://doi.org/10.1073/pnas.1715278115.

Cui, H., Kaufman, A.J., Xiao, S., Peek, S., Cao, H., Min, X., Cai, Y., Siegel, Z., Liu, X.-M., Peng, Y., Schiffbauer, J.D., Martin, A.J., 2016. Environmental context for the terminal Ediacaran biomineralization of animals. Geobiology. https://doi.org/10.1111/gbi.12178.

Dahl, T.W., Boyle, R.A., Canfield, D.E., Connelly, J.N., Gill, B.C., Lenton, T.M., Bizzarro, M., 2014. Uranium isotopes distinguish two geochemically distinct stages during the later Cambrian SPICE event. Earth Planet. Sci. Lett. 401, 313–326. https://doi.org/10.1016/j.epsl.2014.05.043.

Dunk, R.M., Mills, R.A., Jenkins, W.J., 2002. A reevaluation of the oceanic uranium budget for the Holocene. In: Geochemistry of Crustal Fluids—Fluids in the Crust and Chemical Fluxes at the Earth's Surface. Chem. Geol. 190, 45–67. https://doi.org/10.1016/S0009-2541(02)00110-9.

Fike, D.A., Grotzinger, J.P., Pratt, L.M., Summons, R.E., 2006. Oxidation of the Ediacaran Ocean. Nature 444, 744–747. https://doi.org/10.1038/nature05345.

Germs, G.J.B., 1983. Implications of a sedimentary facies and depositional environmental analysis of the Nama group in South West Africa/Namibia. Geol. Soc. S. Afr. 11, 89–114.

Hood, A.v.S., Planavsky, N.J., Wallace, M.W., Wang, X., 2018. The effects of diagenesis on geochemical paleoredox proxies in sedimentary carbonates. Geochim. Cosmochim. Acta 232, 265–287. https://doi.org/10.1016/j.gca.2018.04.022.

Hood, A.v.S., Planavsky, N.J., Wallace, M.W., Wang, X., Bellefroid, E.J., Gueguen, B., Cole, D.B., 2016. Integrated geochemical-petrographic insights from component-selective δ^{238}U of cryogenian marine carbonates. Geology 44, 935–938.

Hua, H., Pratt, B.R., Zhang, L.-Y., 2003. Borings in Cloudina shells: complex predator–prey dynamics in the terminal Neoproterozoic. Palaios 18, 454–459. https://doi.org/10.1669/0883-1351(2003)018.

Hull, P.M., Darroch, S.A.F., Erwin, D.H., 2015. Rarity in mass extinctions and the future of ecosystems. Nature 528, 345–351. https://doi.org/10.1038/nature16160.

Jensen, S., Saylor, B.Z., Gehling, J.G., Germs, G.J.B., 2000. Complex trace fossils from the terminal Proterozoic of Namibia. Geology 28, 143–146.

Kendall, B., Komiya, T., Lyons, T.W., Bates, S.M., Gordon, G.W., Romaniello, S.J., Jiang, G., Creaser, R.A., Xiao, S., McFadden, K., Sawaki, Y., Tahata, M., Shu, D., Han, J., Li, Y., Chu, X., Anbar, A.D., 2015. Uranium and molybdenum isotope evidence for an episode of widespread ocean oxygenation during the late Ediacaran Period. Geochim. Cosmochim. Acta 156, 173–193. https://doi.org/10.1016/j.gca.2015.02.025.

Kimura, H., Watanabe, Y., 2001. Oceanic anoxia at the Precambrian–Cambrian boundary. Geology 29, 995–998.

Lau, K.V., Macdonald, F.A., Maher, K., Payne, J.L., 2017. Uranium isotope evidence for temporary ocean oxygenation in the aftermath of the Sturtian Snowball Earth. Earth Planet. Sci. Lett. 458, 282–292.

Lau, K.V., Maher, K., Altiner, D., Kelley, B.M., Kump, L.R., Lehrmann, D.J., Silva-Tamayo, J.C., Weaver, K.L., Yu, M., Payne, J.L., 2016. Marine anoxia and delayed Earth system recovery after the end-Permian extinction. Proc. Natl. Acad. Sci. 113, 2360–2365.

Lenton, T.M., Daines, S.J., 2018. The effects of marine eukaryote evolution on phosphorus, carbon and oxygen cycling across the Proterozoic–Phanerozoic transition. Emerg. Top. Life Sci. 2 (2), 267–278. https://doi.org/10.1042/ETLS20170156.

Montoya-Pino, C., Weyer, S., Anbar, A.D., Pross, J., Oschmann, W., van de Schootbrugge, B., Arz, H.W., 2010. Global enhancement of ocean anoxia during Oceanic Anoxic Event 2: a quantitative approach using U isotopes. Geology 38, 315–318. https://doi.org/10.1130/G30652.1.

Planavsky, N.J., Reinhard, C.T., Wang, X., Thomson, D., McGoldrick, P., Rainbird, R.H., Johnson, T., Fischer, W.W., Lyons, T.W., 2014. Low mid-Proterozoic atmospheric oxygen levels and the delayed rise of animals. Science 346, 635–638.

Poulton, S.W., Canfield, D.E., 2011. Ferruginous conditions: a dominant feature of the ocean through Earth's history. Elements 7, 107–112. https://doi.org/10.2113/gselements.7.2.107.

Pu, J.P., Bowring, S.A., Ramezani, J., Myrow, P., Raub, T.D., Landing, E., Mills, A., Hodgin, E., Macdonald, F.A., 2016. Dodging snowballs: geochronology of the gaskiers glaciation and the first appearance of the Ediacaran biota. Geology 44, 955–958. https://doi.org/10.1130/G38284.1.

Rolison, J.M., Stirling, C.H., Middag, R., Rijkenberg, M.J.A., 2017. Uranium stable isotope fractionation in the Black Sea: modern calibration of the ^{238}U/^{235}U paleoredox proxy. Geochim. Cosmochim. Acta 203, 69–88. https://doi.org/10.1016/j.gca.2016.12.014.

Romaniello, S.J., Herrmann, A.D., Anbar, A.D., 2013. Uranium concentrations and ^{238}u/^{235}U isotope ratios in modern carbonates from the Bahamas: assessing a novel paleoredox proxy. Chem. Geol. 362, 305–316. https://doi.org/10.1016/j.chemgeo.2013.10.002.

Sahoo, S.K., Planavsky, N.J., Jiang, G., Kendall, B., Owens, J.D., Wang, X., Shi, X., Anbar, A.D., Lyons, T.W., 2016. Oceanic oxygenation events in the anoxic Ediacaran ocean. Geobiology 14, 457–468. https://doi.org/10.1111/gbi.12182.

Sahoo, S.K., Planavsky, N.J., Kendall, B., Wang, X., Shi, X., Scott, C., Anbar, A.D., Lyons, T.W., Jiang, G., 2012. Ocean oxygenation in the wake of the Marinoan glaciation. Nature 489, 546–549. https://doi.org/10.1038/nature11445.

Sperling, E.A., Wolock, C.J., Morgan, A.S., Gill, B.C., Kunzmann, M., Halverson, G.P., Macdonald, F.A., Knoll, A.H., Johnston, D.T., 2015. Statistical analysis of iron geochemical data suggests limited late Proterozoic oxygenation. Nature 523, 451–454. https://doi.org/10.1038/nature14589.

Stirling, C.H., Andersen, M.B., Potter, E.-K., Halliday, A.N., 2007. Low-temperature isotopic fractionation of uranium. Earth Planet. Sci. Lett. 264, 208–225. https://doi.org/10.1016/j.epsl.2007.09.019.

Stirling, C.H., Andersen, M.B., Warthmann, R., Halliday, A.N., 2015. Isotope fractionation of ^{238}U and ^{235}U during biologically-mediated uranium reduction. Geochim. Cosmochim. Acta 163, 200–218. https://doi.org/10.1016/j.gca.2015.03.017.

Stolper, D.A., Keller, C.B., 2018. A record of deep-ocean dissolved O_2 from the oxidation state of iron in submarine basalts. Nature 553, 323. https://doi.org/10.1038/nature25009.

Stylo, M., Neubert, N., Wang, Y., Monga, N., Romaniello, S.J., Weyer, S., Bernier-Latmani, R., 2015. Uranium isotopes fingerprint biotic reduction. Proc. Natl. Acad. Sci. 112, 5619–5624. https://doi.org/10.1073/pnas.1421841112.

Tarhan, L.G., Droser, M.L., Cole, D.B., Gehling, J.G., 2018. Ecological expansion and extinction in the Late Ediacaran: weighing the evidence for environmental and biotic drivers. Integr. Comp. Biol. 58, 688–702. https://doi.org/10.1093/icb/icy020.

Tissot, F.L.H., Dauphas, N., 2015. Uranium isotopic compositions of the crust and ocean: age corrections, U budget and global extent of modern anoxia. Geochim. Cosmochim. Acta 167, 113–143. https://doi.org/10.1016/j.gca.2015.06.034.

Tostevin, R., He, T., Turchyn, A.V., Wood, R.A., Penny, A.M., Bowyer, F., Antler, G., Shields, G.A., 2017. Constraints on the late Ediacaran sulfur cycle from carbonate associated sulfate. Precambrian Res. 290, 113–125. https://doi.org/10.1016/j.precamres.2017.01.004.

Tostevin, R., Wood, R.A., Shields, G.A., Poulton, S.W., Guilbaud, R., Bowyer, F., Penny, A.M., He, T., Curtis, A., Hoffmann, K.H., Clarkson, M.O., 2016. Low-oxygen waters limited habitable space for early animals. Nat. Commun. 7. https://doi.org/10.1038/ncomms12818.

Waggoner, B., 2003. The Ediacaran biotas in space and time. Integr. Comp. Biol. 43, 104–113. https://doi.org/10.1093/icb/43.1.104.

Wei, G.-Y., Planavsky, N.J., Tarhan, L.G., Chen, X., Wei, W., Li, D., Ling, H.-F., 2018. Marine redox fluctuation as a potential trigger for the Cambrian explosion. Geology 46, 587–590. https://doi.org/10.1130/G40150.1.

Weyer, S., Anbar, A.D., Gerdes, A., Gordon, G.W., Algeo, T.J., Boyle, E.A., 2008. Natural fractionation of ^{238}U/^{235}U. Geochim. Cosmochim. Acta 72, 345–359. https://doi.org/10.1016/j.gca.2007.11.012.

Wood, R., Bowyer, F., Penny, A., Poulton, S.W., 2018. Did anoxia terminate Ediacaran benthic communities? Evidence from early diagenesis. Precambrian Res. 313, 134–147. https://doi.org/10.1016/j.precamres.2018.05.011.

Wood, R., Erwin, D.H., 2017. Innovation not recovery: dynamic redox promotes metazoan radiations. Biol. Rev. https://doi.org/10.1111/brv.12375.

Wood, R., Ivantsov, A.Y., Zhuravlev, A.Y., 2017. First macrobiota biomineralization was environmentally triggered. Proc. R. Soc. B 284, 20170059. https://doi.org/10.1098/rspb.2017.0059.

Wood, R.A., Poulton, S.W., Prave, A.R., Hoffmann, K.-H., Clarkson, M.O., Guilbaud, R., Lyne, J.W., Tostevin, R., Bowyer, F., Penny, A.M., Curtis, A., Kasemann, S.A., 2015. Dynamic redox conditions control late Ediacaran ecosystems in the Nama Group, Namibia. Precambrian Res. 261, 252–271.

Zhang, F., Xiao, S., Kendall, B., Romaniello, S.J., Cui, H., Meyer, M., Gilleaudeau, G.J., Kaufman, A.J., Anbar, A.D., 2018. Extensive marine anoxia during the terminal Ediacaran Period. Sci. Adv. 4, eaan8983. https://doi.org/10.1126/sciadv.aan8983.